



UNIVERSITY OF LEEDS

This is a repository copy of *Single-molecule visualization of DNA G-quadruplex formation in live cells*.

White Rose Research Online URL for this paper:  
<http://eprints.whiterose.ac.uk/163757/>

Version: Accepted Version

---

**Article:**

Di Antonio, M, Ponjavic, A [orcid.org/0000-0002-7561-1127](https://orcid.org/0000-0002-7561-1127), Radzevičius, A et al. (8 more authors) (2020) Single-molecule visualization of DNA G-quadruplex formation in live cells. *Nature Chemistry*, 12 (9). pp. 832-837. ISSN 1755-4330

<https://doi.org/10.1038/s41557-020-0506-4>

---

© The Author(s), under exclusive licence to Springer Nature Limited 2020. This is an author produced version of an article published in *Nature Chemistry*. Uploaded in accordance with the publisher's self-archiving policy.

**Reuse**

Items deposited in White Rose Research Online are protected by copyright, with all rights reserved unless indicated otherwise. They may be downloaded and/or printed for private study, or other acts as permitted by national copyright laws. The publisher or other rights holders may allow further reproduction and re-use of the full text version. This is indicated by the licence information on the White Rose Research Online record for the item.

**Takedown**

If you consider content in White Rose Research Online to be in breach of UK law, please notify us by emailing [eprints@whiterose.ac.uk](mailto:eprints@whiterose.ac.uk) including the URL of the record and the reason for the withdrawal request.



[eprints@whiterose.ac.uk](mailto:eprints@whiterose.ac.uk)  
<https://eprints.whiterose.ac.uk/>

1 **Single-molecule visualisation of DNA G-quadruplex formation in live cells.**

2 Marco Di Antonio<sup>1,4†</sup>, Aleks Ponjavic<sup>1,5,6†</sup>, Antanas Radzevičius<sup>1†</sup>, Rohan T. Ranasinghe<sup>1</sup>, Marco  
3 Catalano<sup>1</sup>, Xiaoyun Zhang<sup>1</sup>, Jiazhen Shen<sup>2</sup>, Lisa-Maria Needham<sup>1</sup>, Steven F. Lee<sup>1</sup>, David  
4 Klenerman<sup>1\*</sup>, Shankar Balasubramanian<sup>1,2,3\*</sup>

5  
6 1. Department of Chemistry, University of Cambridge, Cambridge CB2 1EW, UK.

7 2. Cancer Research UK, Cambridge Research Institute, Li Ka Shing Centre, Cambridge CB2  
8 0RE, UK.

9 3. School of Clinical Medicine, University of Cambridge, Cambridge CB2 0SP, UK.

10 4. Current affiliation: Imperial College London, Chemistry Department, Molecular Science  
11 Research Hub, Wood Lane W12 0BZ, London, UK.

12 5. Current affiliation: School of Physics and Astronomy, University of Leeds LS2 9JT, Leeds,  
13 UK.

14 6. Current affiliation: School of Food Science and Nutrition, University of Leeds LS2 9JT, Leeds,  
15 UK.

16

17 † These authors contributed equally to this work.

18

19

20 **Abstract**

21 G-rich sequences can form alternative DNA secondary structures called G-quadruplexes (G4s).

22 Substantial evidence now exists to support that formation of G4 structures is related to gene-  
23 expression and the case for targeting G4s for therapeutic intervention is getting stronger.

24 Nevertheless, there is a need to devise additional approaches to study G4s in living cells to build

25 further understanding on their actual biological relevance. The *in-situ* observation of G4-

26 formation in living cells would provide evidence that goes beyond observations by

27 immunostaining and ChIP-Seq. Herein, we describe a new G4-specific fluorescent probe (SiR-

28 PyPDS) that has properties that enable single-molecule detection of G4s. We use SiR-PyPDS to

29 achieve real-time detection of individual G4 structures in living cells. Live-cell single-molecule

30 fluorescence imaging of G4s is carried out under conditions that use low concentrations of the

31 G4-binding fluorescent probe (20 nM) that enabled us to provide informative measurements

32 representative of the population of G4s in living cells, without globally perturbing G4 formation

33 and dynamics. Single-molecule fluorescence imaging and time-dependent chemical trapping of

34 unfolded G4s in living cells by means of DMS treatment, revealed that G4s fluctuate between

35 folded and unfolded states. We also demonstrated that G4-formation in live cells is cell-cycle

36 dependent and inhibited by chemical inhibition of transcription and replication. The observation

37 of single fluorescent probes binding to individual G4s provides a new experimental perspective

38 on G4-formation and dynamics in living cells. Our imaging approach will help elucidate the

39 putative roles of individual G4s in real-time in the context of living cells.

40

41

## 42 **Introduction**

43 G-quadruplexes (G4s) are non-canonical structures that can form within guanine-rich nucleic acid  
44 sequences (Fig. 1A)<sup>1,2</sup>. Sequencing of G4s in human genomic DNA (G4-Seq) revealed over  
45 700,000 distinct sites that can form G4s, with notable G4-enrichment within gene promoters and  
46 at *loci* commonly amplified in cancers<sup>3</sup>. G4 structures have also been imaged *ex vivo* by  
47 immunofluorescence with G4-selective antibodies, both in fixed ciliates<sup>4</sup> and, more recently, in  
48 fixed human cells<sup>5</sup>. The G4-selective antibody BG4 has been used in chromatin immuno-  
49 precipitation followed by sequencing (ChIP-Seq), showing that just ~1% of the G4s identified in  
50 purified DNA by G4-Seq could be detected within chromatin<sup>6</sup>. ChIP-Seq experiments rely on  
51 measurements integrated over millions of cells and therefore provide only an average view of G4-  
52 incidence at a given genomic *loci*. However, G4 homeostasis in cells is likely to be regulated by  
53 proteins, such as helicases, so *ex vivo* techniques that provide a snapshot of G4 distribution may  
54 hide important dynamic processes that can only be observed by live-cell imaging. Fluorogenic  
55 G4-binding probes for the detection of both RNA<sup>7,8</sup> and DNA<sup>9,10</sup> G4s in living cells have been  
56 reported. Generally, such probes are used at relatively high ( $\mu\text{M}$ ) concentrations which can result  
57 in global induction of G4-structures, perturbation of endogenous G4-folding dynamics and  
58 cellular stress/toxicity through binding to G4s globally. Furthermore, some observational  
59 approaches require environmentally responsive probes which can pose limits on the quantitative  
60 study of specific G4-formation as well the challenge of disentangling genuine G4-binding from  
61 environmental effects. We have pursued single-molecule fluorescence imaging of G4s in living  
62 cells to detect individual G4s in the nucleus of living cells at low nanomolar concentrations of  
63 fluorescent probe. The use of a G4-specific probe (SiR-PyPDS) and a control probe (SiR-  
64 iPyPDS), with poor affinity to G4s, together with ligand competition experiments, confirmed G4s  
65 specificity. Relatively low probe concentrations (nM) helps avoid global induction of G4s  
66 inherent in ensemble fluorescence methods. Specifically, only a small fraction (~4%) of G4s are  
67 bound by the probe, without perturbing global folding dynamics. Herein we report, for the first  
68 time, detection of individual G4s in the nucleus of living human cells by single-molecule  
69 fluorescence microscopy.

## 70 **Results and Discussion**

71 SiR-PyPDS (Fig. 1B) was prepared by tethering the red fluorophore Silicon-Rhodamine (SiR)<sup>11</sup>  
72 to an analogue of an established G4-ligand, pyridostatin<sup>12</sup> (PyPDS), using linkers of different  
73 lengths (Fig. S1 and S2). Upon binding to G4-folded oligonucleotides all SiR-PyPDS analogues  
74 (Fig. S2) displayed a modest fluorescence increase (~10 fold), which is insufficient to confidently  
75 discriminate bound vs unbound probes in cells, but enabled evaluation of optimal linker length by  
76 fluorescence titrations. Binding titrations revealed the six carbon linker of SiR-PyPDS (Fig. 1B)  
77 as being optimal for G4-binding selectivity of the PyPDS-scaffold, with good binding towards  
78 MYC and KIT-1 and h-TELO G4s with  $K_d$  values of 0.63 ( $\pm$  0.08)  $\mu$ M, 1.0 ( $\pm$  0.1)  $\mu$ M and 2.0 ( $\pm$   
79 0.8)  $\mu$ M respectively, and no detectable binding to double- or single-stranded DNA (Fig. S3).  
80 SiR-PyPDS displayed a quantum yield of 0.05 in solution that increases to 0.2 when the molecule  
81 is bound to MYC G4 (see methods). We also designed and synthesized a novel PyPDS isomer  
82 (SiR-iPyPDS, Fig. 1B) that could act as a poor-G4 binding control in live cells experiments to  
83 support unambiguous identification of G4-binding events of SiR-PyPDS. Our control analogue  
84 (SiR-iPyPDS) differs from SiR-PyPDS simply for the position of the amino side-chains on the  
85 quinoline ring. We reasoned that the steric clash of the side-chains in SiR-iPyPDS could prevent  
86 the molecule from adopting the flat conformation required for G-tetrad recognition. Fluorescence  
87 titrations confirmed a more than 10-fold lower G4-binding affinity of SiR-iPyPDS compared to  
88 SiR-PyPDS (Fig. S4).

89 Given the promising results from ensemble binding experiments by SiR-PyPDS and the negative  
90 control analogue SiR-PyPDS, we decided to evaluate the suitability of these probes for single-  
91 molecule detection of G4s *in vitro*. To test this, we investigated the binding of SiR-PyPDS or  
92 SiR-iPyPDS to a G4-folded oligonucleotide, MYC, immobilized on a PEG/biotin-coated surface,  
93 by single-molecule imaging (Fig. 1C-E). We acquired images with a long exposure time (500 ms)  
94 to capture only relatively long-lived interactions. At a much lower ligand concentration than what  
95 was used in ensemble experiments (250 pM), we could detect on average 867 long-lived SiR-  
96 PyPDS spots (Fig. 1F, Supplementary Movie S1) in each field of view (Fig. 1G), but observed a  
97 ten-fold reduction in long-lived binding (66 events,  $P = 5 \times 10^{-6}$ ) for the weaker G4 binder SiR-  
98 iPyPDS (Fig. 1I, Supplementary Movie S1). We confirmed that events represented binding of  
99 individual probes to MYC by observing single-step photobleaching (Fig. S5). As the MYC  
100 sequence was also labelled with Alexa Fluor 488 we could use both FRET (Fig. S6A) and single-  
101 molecule FRET (Fig. S6B-D) to visualize direct binding of our probe to MYC. Note that at 250  
102 pM, the labelled fraction,  $\theta$ , of G4s is about 0.05%, according to the Hill-Langmuir equation  
103  $\theta = [L]/(K_d + [L])$ , where  $[L]$  is the concentration of ligand and  $K_d$  is the dissociation constant

104 for ligand binding to G4s. To further investigate if the number of SiR-PyPDS binding event  
105 correlates with the density of G4 targets immobilized on the surface, we varied the surface  
106 coverage by mixing the biotinylated MYC G4 with a biotinylated single-stranded DNA strand  
107 that does not form a G4, at different ratios (Fig. S7, see Methods). We observed a linear  
108 relationship between the number of SiR-PyPDS binding events detected and the concentration of  
109 MYC G4 immobilised on the surface, confirming that the number of binding events is  
110 proportional to the number of G4s on the surface (Fig. S7) and that this number can be used as a  
111 proxy for G4-density. We have also confirmed that the MYC sequence used is folded into a G4  
112 structure as judged by circular dichroism spectroscopy (Fig. S8). The observed number of binding  
113 events can therefore be used to assess the concentration of folded G4s on the surface. We next  
114 compared the binding of SiR-PyPDS and SiR-iPyPDS to different G4-folding oligonucleotides,  
115 including MYC, h-TELO and c-KIT-1. Again, we observed a >20-fold increase in the number of  
116 binding events for SiR-PyPDS when compared to the control probe SiR-iPyPDS (Fig. S9). These  
117 observations confirm that SiR-PyPDS can be applied to single-molecule imaging of G4s and that  
118 the decreased binding affinity of the control analogue SiR-iPyPDS causes a lower number of  
119 binding events observed (Fig. S9).

120 To further validate that long-lived binding events observed with SiR-PyPDS could be ascribed as  
121 G4-specific, we attempted to compete out SiR-PyPDS binding to MYC G4 with an excess of the  
122 structurally unrelated G4-binding ligand PhenDC3<sup>13</sup>. Gratifyingly, binding of SiR-PyPDS to  
123 MYC was abrogated when an excess (10  $\mu$ M) of the potent G4-ligand PhenDC3 was included as  
124 a competitor (16 events,  $P = 2 \times 10^{-6}$ , Fig. 1F, Supplementary Movie S2). Furthermore, we  
125 measured the number of binding events displayed by SiR-PyPDS when the G4-folding sequence  
126 of MYC was mutated to prevent G4-formation. SiR-PyPDS binding was negligible (23 events,  $P$   
127  $= 2 \times 10^{-6}$ ) for the immobilized single-stranded DNA control (MYC-mut, Fig. 1F, Supplementary  
128 Movie S1), which is in agreement with what was observed for SiR-PyPDS ensemble fluorescence  
129 titrations (Fig. S3). Both the biotin-MYC and MYC-mut used in this experiment were also  
130 functionalized with an Alexa-488 fluorophore. We used the 488 emission to measure the total  
131 fluorescence on each coverslip functionalised with either MYC or MYC-mut to ensure  
132 comparable density of oligonucleotides on the surface between the different experiments ( $\sigma =$   
133 10% variation between coverslips, Fig. S7B). Therefore, differences observed in binding events  
134 were minimally affected by variations in G4 surface coverage, confirming the suitability of SiR-  
135 PyPDS and SiR-iPyPDS control as probes for the single-molecule detection of G4s.

136 We next sought to determine whether the conditions of relatively low probe concentrations used  
137 for single-molecule imaging caused global induction of G4-folding or perturbation of G4-folding  
138 dynamics. To investigate this, we used G4-folding oligonucleotides (MYC, h-TELO and c-KIT1)  
139 labelled with a Cy5 fluorophore at their 5' end and having an overhang hybridised with a  
140 complementary oligonucleotide sequence containing a Cy3 fluorophore at its 3' end. The  
141 oligonucleotides form a Cy3-Cy5 FRET system capable of assessing the fraction of folded G4s  
142 by measuring FRET efficiency between the two fluorophores<sup>14</sup>. When titrated with increasing  
143 concentrations of PyPDS, no significant FRET perturbation was observed for PyPDS  
144 concentrations below 3  $\mu$ M (Fig. S10). Therefore, there is no detectable global induction of G4s  
145 when imaging under single molecule conditions (Fig 1J). We studied G4-unfolding dynamics  
146 using a FRET system with FAM/TAMRA labelled oligonucleotides that were annealed in 150  
147 mM  $K^+$  to form a stable G4 structure (see Methods). We next added a 10 folds molar excess of  
148 DNA sequence complementary to the G4-folding sequence to irreversibly trap the unfolded G4  
149 sequence as dsDNA. This allowed us to measure the unfolding kinetics by monitoring a  
150 concomitant decrease in the FRET fluorescence signal, as previously described<sup>14</sup>. We found that  
151  $\mu$ M concentrations of SiR-PyPDS are required to slow down the unfolding rate for the tested G4s  
152 structures and that low nM concentrations used for single-molecule experiments do not globally  
153 affect the unfolding rate of the tested G4-structures (Table S1). Our data demonstrate that single-  
154 molecule imaging can be used to address the pervasive problem of current G4-detection strategies  
155 that use relatively high concentrations of affinity probes that might globally perturb G4 folding  
156 and dynamics.

157 We next applied the fluorescent G4-ligands to single-molecule imaging of G4s in live cells (Fig.  
158 2A). First, we investigated the toxicity of SiR-PyPDS and SiR-iPyPDS in U2OS cells over a 24 h  
159 treatment at different probe concentrations. Both SiR-PyPDS and SiR-iPyPDS did not elicit any  
160 cell death response at nM concentrations, as toxicity could only be observed at concentrations  
161 higher than 10  $\mu$ M (Fig. S11). Based on this, U2OS cells were treated for 30 min with 20 nM of  
162 SiR-PyPDS, which resulted in under-labeling of G4s at a density where individual fluorophores  
163 were spatially well separated (Fig. 2B). This allowed us to visualize individual probes (SiR-  
164 PyPDS or SiR-iPyPDS) binding to targets in the nucleus (Fig. 2B-C, Supplementary Movie S3)  
165 using single-molecule imaging (400 frames taken with 100 ms exposure using highly inclined  
166 laminated optical sheet (HILO) microscopy)<sup>15</sup>. Single step photobleaching provided evidence of  
167 binding events by individual probe molecules in the nucleus (Fig. S12), in spite of the extra-  
168 nuclear lysosomal accumulation of SiR-PyPDS (Fig. S13). We first measured the number of

169 binding events whereby a SiR-PyPDS molecule remained stationary within a 300 nm radius for  
170 three or more consecutive frames (i.e. 300 ms), detecting an average of 79 binding events per  
171 nuclei (Fig. 2D). Similarly to what was observed *in vitro*, treatment of U2OS cells with SiR-  
172 iPyPDS (20 nM) revealed an average of only 2 long-lived binding events in the nucleus (Fig. 2D).  
173 To confirm that differences in the number of nuclear binding events between SiR-PyPDS and  
174 SiR-iPyPDS were not due to different cellular uptake of the two ligands, we used confocal  
175 microscopy and demonstrated that upon 10  $\mu$ M ligands treatment the total nuclear fluorescence  
176 intensity measured was comparable between the SiR-PyPDS and SiR-iPyPDS treatments (Fig.  
177 S14). These results are consistent with the *in vitro* observations (Fig. 1F) and corroborate the  
178 hypothesis that long-lived SiR-PyPDS binding events could be ascribed to specific G4-binding in  
179 cells. To further support this hypothesis, we demonstrated that SiR-PyPDS binding could be  
180 abrogated in the presence of 10  $\mu$ M of the unlabeled competitor G4-ligands PDS<sup>12</sup> or PhenDC3<sup>13</sup>  
181 (Fig. S15, Supplementary Movie S4), which is also consistent with what was observed *in vitro*.

182 We next sought to estimate the fraction of G4-labelled by SiR-PyPDS in living cells as we have  
183 done for the *in vitro* studies. To do so, we have assumed that the  $K_d$  of SiR-PyPDS remains  
184 unchanged in the cellular environment and that the nuclear concentration of the probe is 20 nM.  
185 Based on these assumptions and using the relationship  $[L]/(K_d + [L])$ , the fraction of labelled  
186 G4s on a single U2OS cells is around 4%. Using this value for labelled G4 fraction, we have  
187 roughly estimated the total number of G4s present in a single cell. As we detect about 10 binding  
188 events on average in an image frame within a single focal plane ( $\sim 1\mu$ m), there would be around  
189 100 binding events in an entire U2OS cell of diameter  $\sim 10\mu$ m. Therefore, considering we are  
190 labelling around 4% of the total number of targets, we can estimate a total number of G4s in a  
191 single cell of  $\sim 3000$ , which is in line with what has been detected in human chromatin (between  
192 1,000 and 10,000 G4s) by G4-ChIP-Seq experiments.<sup>6</sup>

193 We then compared the temporal dynamics of the interaction between SiR-PyPDS and G4s *in vitro*  
194 and in cells, to investigate if characteristic dwell times of SiR-PyPDS binding to G4s *in vitro*  
195 could also be detected in cells. Time-lapse imaging was used to observe long-lived events (Fig.  
196 3A, Supplementary Movie S5). *In vitro*, an exposure time of 100 ms and interval of 2 s was used  
197 to avoid photobleaching effects (time constant  $\tau_b = 923$  s), whereas for cellular experiments a  
198 slightly longer interval (3 s,  $\tau_b = 104$  s) and also a longer exposure time (500 ms) were needed to  
199 limit contributions from unbound ligands<sup>16</sup>. The histogram of SiR-PyPDS dwell times could be  
200 well fitted ( $R^2 > 0.99$ ) to a single exponential distribution, yielding a photobleaching-corrected  
201 binding lifetime of  $6.6 \pm 0.5$  s in cells (Fig. 3B), which is significantly shorter ( $\sim 2.5$  folds,  $P =$

202  $4 \times 10^{-7}$ , unpaired t-test) than that observed *in vitro* for binding ( $15.4 \pm 0.6$  s) to MYC G4. To  
203 investigate further this apparent discrepancy, we carried out *in vitro* binding experiments with  
204 other G4-forming sequences. These experiments indicated that the dwell times for SiR-PyPDS  
205 binding to hTelo and c-KIT1 were respectively 2.5 and 2 times shorter than MYC and were  
206 comparable to dwell times observed in living cells. These experiments suggested that the binding  
207 dynamics of SiR-PyPDS to synthetic G4-forming oligonucleotides observed *in vitro* can be  
208 recapitulated in cells, further supporting that our assay can detect endogenous G4s.

209 To gain insight into G4-folding dynamics in living cells, we employed the DNA-methylating  
210 agent dimethyl-sulfate (DMS) to irreversibly trap the unfolded G4 state (Fig. 3C). The  
211 nucleophilic N7 atoms of guanines are exposed and can be methylated by DMS in single- and  
212 double-stranded DNA, but are protected in folded G4s by their participation in Hoogsteen  
213 hydrogen bonding (Fig 1A). Thus, transiently unfolded G4s can be methylated and irreversibly  
214 prevent further G4 re-folding by blocking Hoogsteen hydrogen bonding at N7s (Fig. 3C). First,  
215 we demonstrated that DMS could trap the unfolded G4 state *in vitro* by quantifying binding  
216 events of SiR-PyPDS with MYC prior to (300 events) and after (40 events,  $P = 0.03$ ) 20 min  
217 treatment with 640 mM (8%) DMS (Fig. 3D). We then examined if a similar DMS-dependent G4  
218 depletion could be recapitulated in living cells, while keeping the DMS concentration lower (20  
219 mM, 0.25%) to prevent cell death. We observed a time-dependent decrease of SiR-PyPDS  
220 binding events in U2OS cells within minutes after DMS treatment (Fig 3E, Supplementary Movie  
221 S6), with a ~20-fold reduction ( $P = 0.006$ ) in binding events after 20 min exposure. These results  
222 suggest that G4s naturally undergo structural fluctuations in cells. This, in turn, makes their  
223 specific detection by chemical methods, such as DMS-Seq<sup>17</sup>, ineffective, as they will inevitably  
224 trap the unfolded state (Fig. 3C).

225 We further probed dynamic formation of G4s in live U2OS cells through different phases of the  
226 cell cycle to gain insights into changes in G4-prevalence during active DNA processing states,  
227 such as replication (S phase) and transcription (G1 phase). We first confirmed using confocal  
228 microscopy that under different conditions tested there were negligible differences in uptake of  
229 the fluorescent G4 ligand (Fig. S14). This ensured that the lack of binding events observed under  
230 certain cycle phases or after DMS treatment could be confidently ascribed to a change in G4  
231 prevalence. SiR-PyPDS-treated U2OS cells were synchronized to S, G1/S and G0/G1 phases  
232 using previously reported procedures<sup>4</sup> and imaged using single-molecule fluorescence  
233 microscopy. During S phase, where the cell is undergoing active replication, significant ( $P < 10^{-6}$ )  
234 binding events could be detected (208 events, Fig. 4A, Supplementary Movie S7). The number of



235 binding events was slightly reduced (103 events,  $P = 0.01$ ) when cells are preparing to initiate  
236 replication (G1/S phase) and transcription is active (Fig. 4B, Supplementary Movie S7). There  
237 were negligible ( $P < 10^{-6}$ ) binding events during G0/G1 phase (3 events, Fig. 4C, Supplementary  
238 Movie S7), where cellular processes are quiescent. These results show that G4 formation is  
239 associated with both transcription and replication and is in agreement with previous observations  
240 reported in fixed cells<sup>4,18</sup>. To further confirm the suppression of G4s in the absence of actively  
241 processed DNA, we treated unsynchronized U2OS cells with a global replication inhibitor  
242 aphidicolin and also the global transcription inhibitor DRB as previously described<sup>17</sup>, in order to  
243 mimic the quiescent state that characterizes cells undergoing G0 phase. Upon transcription and  
244 replication arrest few binding events were detected (3 events,  $P < 10^{-6}$ ), further demonstrating that  
245 actively processed DNA is pivotal for G4 formation in living cells (Fig. 4C-D, Supplementary  
246 Movie S7).

## 247 **Conclusions**

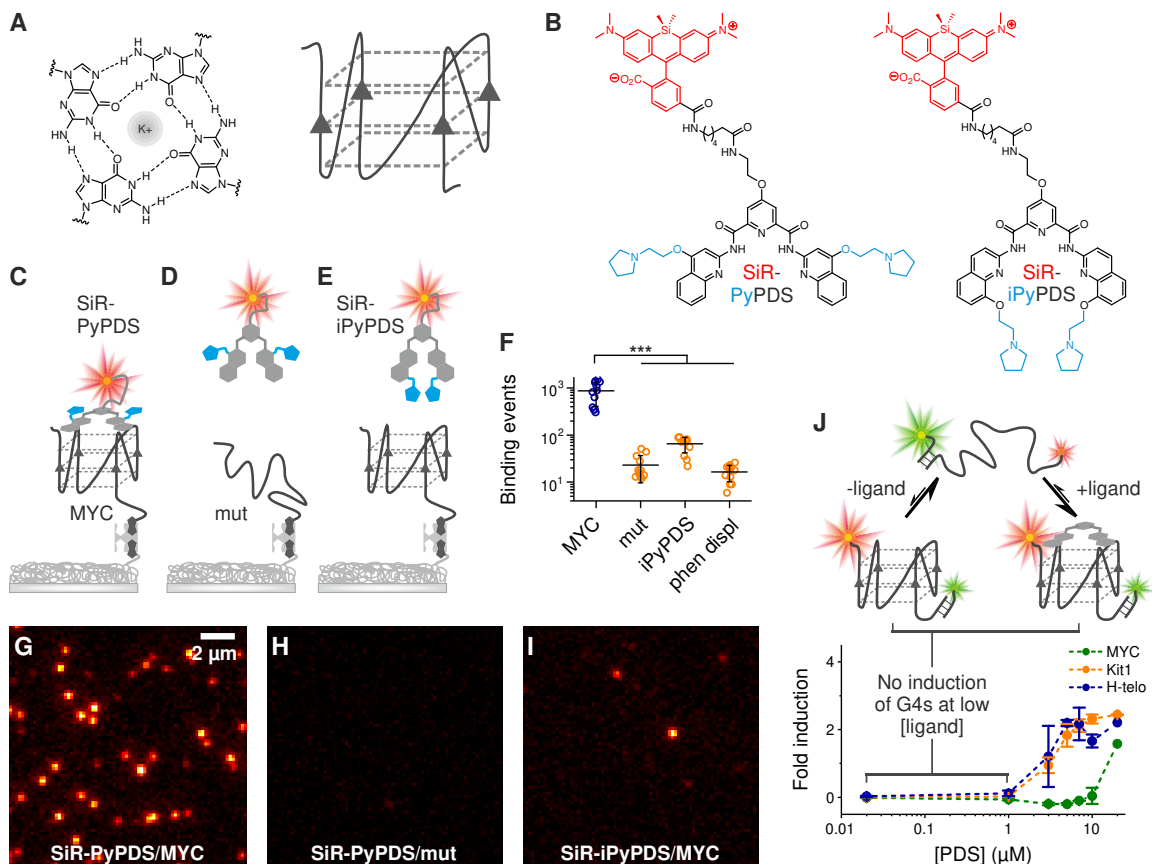
248 We have used fluorescent probe molecules to visualise individual G4 structures in living cells, for  
249 the first time, using single-molecule fluorescence imaging. The sensitivity of single-molecule  
250 methods enabled us to image single binding events to G4 structures at probe concentrations  
251 orders of magnitude lower than normally used in biophysical and cellular experiments, thereby  
252 minimizing global perturbation of G4s. We applied our new imaging platform to demonstrate that  
253 G4-formation is cell-cycle dependent and that the presence of G4s is directly related to  
254 fundamental biological processes such as active transcription and replication, as chemical  
255 inhibition of these processes led to abrogation of detectable G4s in living cells. Trapping of  
256 unfolded G4s by means of DMS methylation revealed that G4s undergo dynamic fluctuations in  
257 live cells and that essentially all G4s are trapped in the unfolded state during the course of 20 min  
258 DMS treatment (0.25%, 20 mM). We anticipate that further application of this imaging platform  
259 will help unravel specific biological functions regulated by individual G4s within the human  
260 genome in real-time.

261 **Supplementary Information** is available in the online version of the paper.

262 **Acknowledgements** Supported by programme grant funding from Cancer Research UK  
263 (C9681/A18618, S.B.) core funding from Cancer Research UK (C14303/A17197, S.B.), a Royal  
264 Society University Research Fellowship (UF120277 to S.F.L.), Research Professorship  
265 (RP150066 to D.K.), a EPSRC (EP/L027631/1 to D.K.) and a BBSRC David Phillips Fellowship  
266 (BB/R011605/1 to M.D.A)

267 **Author Contributions** M.D.A. performed the design, synthesis and biophysical characterization  
268 of G4 ligands. A.P. developed the optical setups used for imaging. M.D.A., A.P. and R.T.R.  
269 performed *in vitro* imaging experiments. R.T.R. carried out surface preparation for *in vitro*  
270 experiments. M.D.A. and A.P. performed imaging experiments in cells. A.P. analyzed imaging  
271 data. M.C. A.R. and X.Z. contributed to the synthesis and biophysical validation of the ligands.  
272 M.D.A., A.P., R.T.R., S.F.L., D.K. and S.B. contributed to the study design. J.S. assisted with  
273 DMS experiments. A.R. contributed to cellular staining and imaging. A.R and L.N characterized  
274 the fluorescence properties of the G4 ligands. M.D.A., A.P., D.K. and S.B. interpreted the results  
275 and co-wrote the manuscript with input from all authors.

276 **Author information:** The data reported in this paper is available in the main text or in the  
277 supporting information. Reprints and permissions information is available at  
278 [www.nature.com/reprints](http://www.nature.com/reprints). S.B. is a founder and shareholder of Cambridge Epigenetix Ltd.  
279 Correspondence and requests for materials should be addressed to S.B. ([sb10031@cam.ac.uk](mailto:sb10031@cam.ac.uk))  
280 and D.K. ([dk10012@cam.ac.uk](mailto:dk10012@cam.ac.uk)).  
281

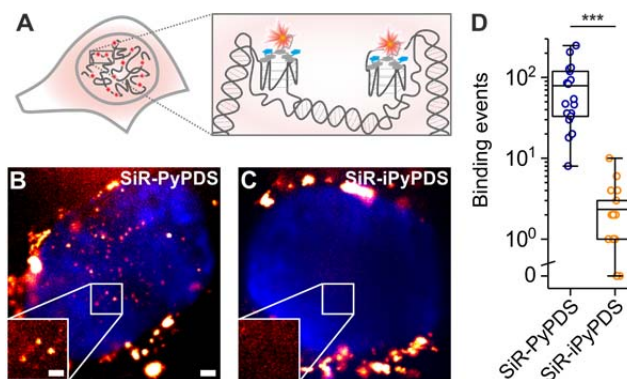


282

283 **Figure 1. *In vitro* single-molecule fluorescence imaging of G-quadruplexes.** (A) Schematic  
 284 representation of a G-tetrad (left) and a G4 structure (right). (B) Chemical structure of the  
 285 selective G4-fluorogenic ligand SiR-PyPDS (left) and its inactive isomer, SiR-iPyPDS (right).  
 286 (C) Schematic of methodology used for visualizing individual G4s. Pre-folded G4 MYC is  
 287 attached to a coverslip via a biotin-neutravidin linker. The fluorescent G4-probe SiR-PyPDS  
 288 binds to G4 MYC, which can be visualized using single-molecule fluorescence imaging. (D) SiR-  
 289 PyPDS will not bind single stranded mutated-MYC that cannot form a G4. (E) The inactive  
 290 isomer SiR-iPyPDS with its 10 times reduced binding affinity is less likely to bind G4 MYC. (F)  
 291 Quantification of SiR-PyPDS binding to the G4 MYC ii) SiR-PyPDS binding to the mutated-  
 292 MYC; iii) SiR-iPyPDS binding to the G4 MYC; iv) SiR-PyPDS binding to the G4 MYC in the  
 293 presence of 10  $\mu\text{M}$  unlabeled PhenDC3 competitor. Error bars indicate mean  $\pm$  sd. \*\*\*  $P < 10^{-5}$ ,  
 294 unpaired t-test. (G) Representative images (500 ms exposure) of individual SiR-PyPDS  
 295 molecules (250 pM) binding to a surface coated with pre-folded MYC G4 oligonucleotide;  
 296 individual fluorescent puncta indicate binding of single SiR-PyPDS molecules. (H) SiR-PyPDS  
 297 (250 pM) binding to mutated-MYC. (I) SiR-iPyPDS (250 pM) binding to pre-folded MYC. (J)  
 298 Interactions of G4 ligands and G4s can alter the equilibrium between unfolded and folded G4s.

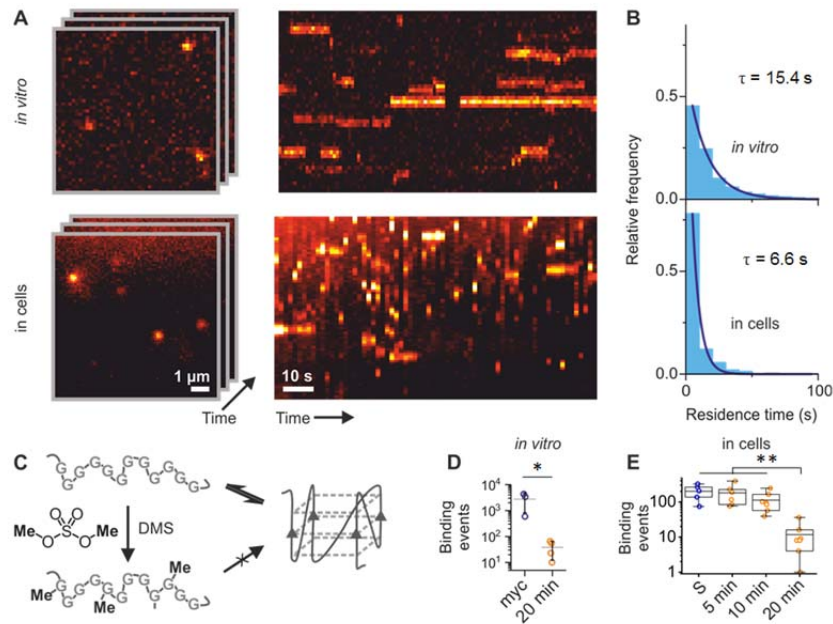
299 Changes in the FRET ratio can be observed at  $\mu\text{M}$  PDS concentrations for Kit1 and hTelo and  
300 larger concentrations for MYC, indicative of G4 induction, which does not occur at lower  
301 concentrations.

302



303

304 **Figure 2. Single-molecule fluorescence imaging of G-quadruplexes in living cells using the**  
305 **fluorescent probe SiR-PyPDS.** (A) Schematic of G4s in the cell nucleus with a zoom-in  
306 showing G4s stained by SiR-PyPDS. (B) Representative background-subtracted image (max  
307 projection of 100 frames with 200 ms exposure) of SiR-PyPDS binding events in a living U2OS  
308 cell treated with 20 nM SiR-PyPDS for 30 min before imaging; fluorescent puncta indicate  
309 binding of single SiR-PyPDS molecules. Blue color corresponds to nuclear staining with Hoechst  
310 33342. Scale bar is 2  $\mu\text{m}$ . Inset scale bar is 1  $\mu\text{m}$ . (C) Representative image of SiR-iPyPDS  
311 staining in living U2OS cell treated with 20 nM SiR-PyPDS for 30 min before imaging. (D)  
312 Quantification of the binding events within the nucleus lasting more than one frame (100 ms per  
313 frame) per cell for SiR-PyPDS and SiR-iPyPDS. Center lines indicate the median; boxes show  
314 interquartile range; whiskers denote 5<sup>th</sup> and 95<sup>th</sup> percentiles. \*\*\*  $P < 10^{-5}$ , Mann-Whitney U-test.



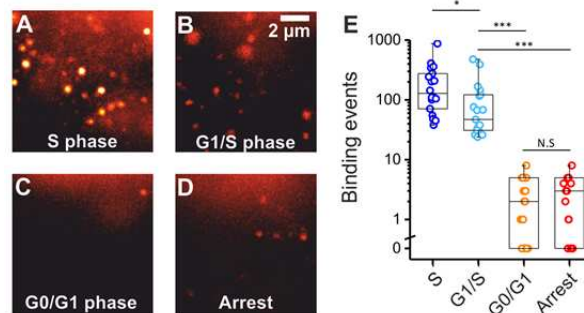
315

316 **Figure 3. G-quadruplexes in living cells undergo dynamic folding/unfolding.** (A) Single-  
 317 molecule time-lapse imaging of SiR-PyPDS *in vitro* (top) and in cells (bottom). Individual images  
 318 from the time-lapse stack are shown on the left and kymographs on the right show the dynamic  
 319 binding kinetics of SiR-PyPDS to G4s. (B) The histograms of dwell times for each experiment (3  
 320 positions on a cover slip for *in vitro* and 6 cells for the cell experiment) were fitted with a single-  
 321 exponential fit to determine the binding lifetime in each condition. (C) Schematic of DMS-  
 322 mediated chemical trapping of unfolded G4s. (D) Quantification of G4-binding events for  
 323 untreated and 600 mM DMS-treated G4 MYC for 20 min. Error bars indicate mean  $\pm$  sd. \*  $P <$   
 324 0.05, Mann-Whitney U-test. (E) Quantification of G4-binding events detected in living cells upon  
 325 increased exposure to DMS (20 mM), showing a clear time-dependent depletion of G4s. Center  
 326 lines indicate the median; boxes show interquartile range; whiskers denote 5<sup>th</sup> and 95<sup>th</sup>  
 327 percentiles. \*\*  $P <$  0.01, Mann-Whitney U-test.

328

329

330



331

332

333 **Figure 4. The observation of G4s in live cells is altered by the cell cycle phase and**  
 334 **transcription.** Representative single-molecule images of G4-binding events are shown for  
 335 synchronized U2OS cells in (A) the S phase, (B) the G1/S phase, (C) the G0/G1 phase and (D)  
 336 for unsynchronized cells treated with both the transcriptional inhibitor DRB and the replication  
 337 inhibitor Aphidicolin. (E) Quantification of binding events lasting more than two frames (100 ms  
 338 per frame) per cell in living U2OS cells at different cell-cycle phases and after  
 339 transcription/replication arrest. Center lines indicate the median; boxes show interquartile range;  
 340 whiskers denote 5<sup>th</sup> and 95<sup>th</sup> percentiles. \*\*\* P < 10<sup>-5</sup>, \* P < 0.05, N.S P > 0.95 Mann-Whitney U-  
 341 test.

342

343

### 344 **Methods**

345 Detailed synthetic protocols and purification methodologies for the preparation of SiR-PyPDS  
 346 and SiR-iPyPDS, biophysical methods and more detailed protocols are described in supporting  
 347 information.

348

### 349 ***In vitro* single-molecule fluorescence imaging**

350 Binding of G4 ligands to synthetic biotinylated oligonucleotides was imaged at single-molecule  
 351 resolution by total internal reflection fluorescence microscopy (TIRFM) on glass coverslips  
 352 coated with polyethylene glycol (PEG) and NeutrAvidin. In this study, we used two different  
 353 PEG coating procedures (see SI): one based on passive adsorption (Coating method 1, used for  
 354 data in Fig. 1, 3 and S5) and the other on covalent coupling (Coating method 2, used for data in  
 355 Fig. S6, S7 and S9). We found similar surface densities of immobilized biotinylated  
 356 oligonucleotides and degrees of non-specific binding on each surface. Buffers for surface  
 357 treatment and imaging were freshly filtered each day (0.02 μm syringe filter, Whatman, Cat. No.

358 6809–2101). Each biotinylated surface was then treated in the same way prior to single-molecule  
359 imaging. Wells were first coated with 10  $\mu$ L of 0.2 mg/mL NeutrAvidin (ThermoFisher, Cat. No.  
360 31000) in 1x PBS containing 0.05% tween-20 for 5 min, washed twice with 10  $\mu$ L of 1x PBS  
361 containing 0.05% tween-20, then treated with 10  $\mu$ L of 1x PBS containing 1% tween-20 for 10  
362 min. Biotinylated oligonucleotides (c-MYC or c-MYC-mutant, annealed overnight at 100 nM  
363 concentration in 100 mM KCl and 50 mM KH<sub>2</sub>PO<sub>4</sub>, pH 7.4) were then diluted to 10 nM in 1x  
364 PBS containing 0.05% tween-20 and 10  $\mu$ L added to each well for 5 min. The wells were then  
365 washed twice with 10  $\mu$ L of 1x PBS containing 0.05% tween-20, then treated with 10  $\mu$ L of 1x  
366 PBS containing 1% tween-20 for 10 min. The wells were then washed once with 250 pM of G4  
367 ligand solutions (SiR-PyPDS or SiR-iPyPDS) in PBS and the solution was finally replaced with 9  
368  $\mu$ L of G4 ligand at 250 pM in PBS. For *in vitro* ligand displacement experiments, 1  $\mu$ L of 1mM  
369 PhenDC3 was added to the well. For DMS trapping the pre-annealed MYC oligonucleotide (100  
370 nM) was treated with DMS 8% for 20 minutes, quenched by adding 10%  $\beta$ -mercapto-ethanol and  
371 used for surface coating.

372

373 The general setup used for TIRFM has been described previously<sup>19</sup>. For the *in vitro* experiments  
374 TIRFM was implemented on a Nikon Eclipse Ti2 inverted microscope with a Perfect Focus  
375 System for maintaining focus during acquisition. 488 nm (MLD 488-200, Cobolt) and 640 nm  
376 (LBX-638-180-CSB-PP, Oxxius) lasers were used for excitation with clean-up filters. The  
377 emission collected by the 1.49 NA oil immersion 60 $\times$  (90 $\times$  with internal magnification) objective  
378 lens (Nikon) was filtered with long-pass and band-pass filters (520/36 – 67030 and 692/40 –  
379 67038, Edmund Optics) and imaged on an Evolve 512 Delta EMCCD (Photometrics) with a pixel  
380 size of 178 nm, confirmed using a Ronchi ruling. The excitation power density was measured by  
381 determining the excitation power after the objective and the beam size in the imaging plane,  
382 taking  $\sim$ 4-fold near-field enhancement into account. For binding event measurements, a field of  
383 view was acquired for each condition with 500 ms exposure time at a power density of 1.4  
384 kW/cm<sup>2</sup>. For longer residency time measurements, time lapses of 300 frames were acquired every  
385 2 s with an exposure time of 100 ms and a power density of 0.4 kW/cm<sup>2</sup>. For shorter residency  
386 time measurements, time lapses of 300 frames were acquired every 100 ms with an exposure time  
387 of 100 ms and a power density of 0.4 kW/cm<sup>2</sup>.

388

### 389 **Live Cell Imaging**

390 In a typical experiment  $\sim$ 200,000 U2OS cells diluted in 2 ml of DMEM were plated in a 35 mm  
391 dish with a 14mm Glass coverslip at the bottom (MatTek) and allowed to adhere overnight. After

392 ~18h, the media was replaced with 2 ml of fresh DMEM media containing SiR-PyPDS or SiR-  
393 iPyPDS at a final concentration of 20 nM and cells were further incubated for 30 min. The  
394 DMEM media containing SiR molecules was then discarded and cells were washed 2X with PBS  
395 pre-warmed at 37 °C. Finally, the media was replaced with PBS containing Hoechst 2µM for  
396 nuclear staining, pre-warmed at 37 °C, which was immediately followed by imaging.

397 The effect of DMS on cellular G4 prevalence was evaluated by treatment prior to SiR-PyPDS  
398 labelling: cells were incubated with DMEM containing 20 mM DMS for the indicated time (5, 10  
399 or 20 min). After the desired treatment time DMS was quenched by adding 10% β-mercapto-  
400 ethanol in PBS followed by 2X washing with PBS pre-warmed at 37 °C.

401 Cell cycle synchronisation was performed with mimosine treatment as previously described<sup>4</sup>.  
402 Transcriptional and replication arrest was achieved by co-treatment of cells with DRB and  
403 Aphidicolin as previously described<sup>17</sup>.

404

405 Binding of SiR-PyPDS to nuclear G4s was visualised using highly inclined laminated optical  
406 sheet (HILO) microscopy<sup>15</sup>. The microscope setup used has been described previously<sup>20</sup>. The  
407 central plane of the nucleus in U2OS cells was found with either bright-field microscopy or using  
408 Hoechst staining. For binding event measurements, 400 frames were acquired for each cell with  
409 100 ms exposure time at a power density of 180 W/cm<sup>2</sup>. For residency time measurements, time  
410 lapses of 70 frames were acquired every 3 s with an exposure time of 500 ms and a power density  
411 of 180 W/cm<sup>2</sup>.

412

#### 413 **References:**

- 414 1. Sen, D., Gilbert, W. Formation of parallel four-stranded complexes by guanine-rich  
415 motifs in DNA and its implications for meiosis. *Nature* **334**, 364-366 (1988).
- 416 2. Hänsel-Hertsch, R., Di Antonio, M., Balasubramanian, S. DNA G-quadruplexes in  
417 the human genome: detection, functions and therapeutic potential. *Nat. Rev. Mol. Cell*  
418 *Biol.* **18**, 279-284 (2017).
- 419 3. Chambers, V. S., Marsico, G., Boutell, J. M., Di Antonio, M., Smith, G. P.,  
420 Balasubramanian, S. High-throughput sequencing of DNA G-quadruplex structures in  
421 the human genome. *Nat. Biotechnol.* **33**, 877-881 (2015).
- 422 4. Schaffitzel, C., Berger, I., Postberg, J., Hanes, J., Lipps, H.J., Plückthun, A. In vitro  
423 generated antibodies specific for telomeric guanine-quadruplex DNA react with  
424 *Stylonychia lemnae* macronuclei. *Proc. Natl. Acad. Sci U. S. A.* **98**, 8572-8577  
425 (2001).
- 426 5. Biffi, G., Tannahill, D., McCafferty, J., Balasubramanian, S. Quantitative  
427 visualization of DNA G-quadruplex structures in human cells. *Nat. Chem.* **3**, 182-186  
428 (2013).



- 429 6. Hänsel-Hertsch, R. *et al.* G-quadruplex structures mark human regulatory chromatin.  
430 *Nat. Genet.* **48**, 1267-1272 (2016).
- 431 7. Chen, X. C. *et al.* Tracking the dynamic folding and unfolding of RNA G-  
432 quadruplexes in live cells. *Angew. Chem. Int. Ed.* **57**, 4702–4706 (2018).
- 433 8. Laguerre, A. *et al.* Visualization of RNA G-quadruplexes in live cells. *J. Am. Chem.*  
434 *Soc.* **137**, 8521–8525 (2015).
- 435 9. Zhang, S. *et al.* Tang, Real-time monitoring of DNA G-quadruplexes in living cells  
436 with a small-molecule fluorescent probe. *Nucleic Acids Res.* **46**, 7522-7532 (2018).
- 437 10. Shivalingam, A. *et al.* The interactions between a small-molecule and G-  
438 quadruplexes are visualized by fluorescence lifetime imaging microscopy. *Nat.*  
439 *Commun.* **6**, 8178 (2015).
- 440 11. Lukinavičius, G. *et al.* A near-infrared fluorophore for live-cell super-resolution  
441 microscopy of cellular proteins. *Nat. Chem.* **5**, 132-139 (2013).
- 442 12. Rodriguez, R., Müller, S., Yeoman, J. A., Trentesaux, C., Riou, J. F.,  
443 Balasubramanian, S. A novel small molecule that alters shelterin integrity and  
444 triggers a DNA-damage response at telomeres. *J. Am. Chem. Soc.* **130**, 15758–15759  
445 (2008).
- 446 13. De Cian, A., Delemos, E., Mergny, J. L., Teulade-Fichou, M. P., Monchaud, D.  
447 Highly efficient G-quadruplex recognition by bisquinolinium compounds. *J. Am.*  
448 *Chem. Soc.* **129**, 1856–1857 (2007).
- 449 14. Ying, L., Green, J. J., Li, H., Klenerman, D., Balasubramanian, S. Studies on the  
450 structure and dynamics of the human telomeric G-quadruplex by single-molecule  
451 fluorescence resonance energy transfer. *Proc. Natl. Acad. Sci U. S. A.* **100**, 14629-  
452 14634 (2003).
- 453 15. Tokunaga, M., Imamoto, N., Sakata-Sogawa, K. Highly inclined thin illumination  
454 enables clear single-molecule imaging in cells. *Nat. Methods* **5**, 159-161 (2008).
- 455 16. Etheridge, T. J. *et al.* Quantification of DNA-associated proteins inside eukaryotic  
456 cells using single-molecule localization microscopy. *Nucleic Acids Res.* **42** e146  
457 (2014).
- 458 17. Guo, J. U., Bartel, D.P. RNA G-quadruplexes are globally unfolded in eukaryotic  
459 cells and depleted in bacteria. *Science* **353**, pii: aaf537 (2016).
- 460 18. Rodriguez, R. *et al.* Small-molecule-induced DNA damage identifies alternative  
461 DNA structures in human genes. *Nat. Chem. Biol.* **8**, 301-310 (2012).
- 462 19. Ponjavic, A. *et al.* Single-Molecule Light-Sheet Imaging of Suspended T Cells.  
463 *Biophys. J.* **114**, 2200-2211 (2018).
- 464 20. Ponjavic, A., Ye, Y., Laue, E., Lee, S. F., Klenerman, D. Sensitive light-sheet  
465 microscopy in multiwell plates using an AFM cantilever. *Biomed. Opt. Express* **9**,  
466 5863-5880 (2018).
- 467